Journal of Computational and Applied Mechanics, Vol. 5., No. 1., (2004), pp. 33–48

FINITE ELEMENT ANALYSIS OF STRUCTURES ON THE BASE OF HETEROGENEOUS MODELS

László Ecsi and Pál Élesztős
Faculty of Mechanical Engineering, Slovak University of Technology in Bratislava
Námestie slobody 17, 812 31 Bratislava 1, Slovak Republic
ladislav.ecsi@stuba.sk, pavel.elesztos@stuba.sk

[Received: October 13, 2003]

Abstract. In the paper a simple fracturing model is presented using the 2D discrete element method capable of simulating large-scale brittle fracturing. It uses the combined Mohr-Coulomb and Rankine material model and mode I fracturing in the Rankine corner based on the rotating crack model. In the interactions between the bodies, the Coulomb friction model is considered by using a contact interface element and utilizing the penalty method in its formulation. The modified central difference scheme is used to solve the above explicit dynamic problem.

Mathematical Subject Classification: 74R99, 74S05
Keywords: DEM, brittle fracturing, multi-surface plasticity and softening, explicit dynamic formulation, Coulomb friction contact

1. Introduction

Fracturing simulation presents a challenging task in mechanical engineering. There are various approaches [5], [11] to describe and solve the above problem, however none of their applicabilities is in general straightforward. One of the methods to simulate fracturing is the Discrete Element Method (DEM). Its attractiveness lies first of all in its relatively easy mathematical formulation and computational implementation, and it requires for its material model only a few parameters, which are in general easily measurable. The DEM is an extension of the Finite Element Method (FEM). It can be considered to be a FEM enriched by the contact between the discrete bodies. Due to the contact and the possible softening in the material model and to the possibility of having an unconstrained body among the discrete bodies during the calculation, it requires an explicit dynamic formulation and corresponding central difference scheme for its solution.

2. Mathematical formulation

2.1. **The node facet contact based on the penalty method.** The most essential part of the DEM is the contact formulation [1],[6]. The contact problem can be

©2004 Miskolc University Press

viewed as a specific restraint imposition problem of the discretised continuum system of bodies in contact. The most widespread method in restraint imposition is the penalty method. The potential energy increase corresponding to the contact (see also Figure 1) can be written as follows:

$$\delta A^c = \delta \left(\frac{1}{2} \alpha_n g_n^2 + \frac{1}{2} \alpha_t g_t^2 \right), \tag{2.1}$$

where $\alpha_n, \alpha_t, g_n, g_t$ are the normal (tangential) penalties and actual normal (tangential) gaps.

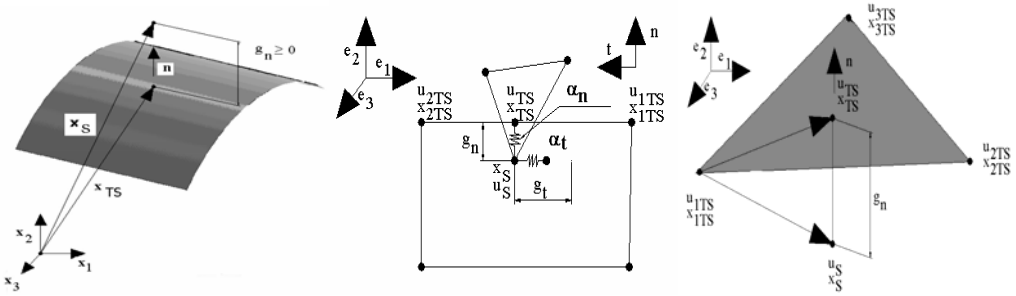

Figure 1. Positive sign convention and node to facet contact 2D and 3D implementation

The principle of minimum potential energy states the contact internal force vector as the first derivative of the contact potential energy according to the contact displacement vector given by the following formula:

$$\mathbf{f}_c^{\text{int}} = \frac{\partial A^c}{\partial \mathbf{u_c}} = \alpha_n g_n \frac{\partial g_n}{\partial \mathbf{u_c}} + \alpha_t g_t \frac{\partial g_t}{\partial \mathbf{u_c}} = \mathbf{f}_{c_n}^{\text{int}} + \mathbf{f}_{c_t}^{\text{int}}. \tag{2.2}$$

2.1.1. *Normal and tangential gap calculation and discretization.* The discretization of the system requires defining a pair of contact nodes given by the Euler coordinates $\mathbf{x_S}$ of a contractor node and the corresponding target or defense node given by $\mathbf{x_{TS}}$ as a normal projection of the contractor node to the facet. By using shape functions, Lagrange coordinates and deflections for the actual normal and tangential gaps, the following expressions can be written:

$$g_n = (\mathbf{x_S} - \mathbf{x_{TS}}) \cdot \mathbf{n} = (\mathbf{X_S} + \mathbf{u_S} - \sum_{i=1}^{n_{facet}} N_i(\mathbf{X_i} + \mathbf{u_i})) \cdot \mathbf{n}, \tag{2.3}$$

$$g_t = (\mathbf{x_S} - \mathbf{x_{TS}}) \cdot \mathbf{t} = (\mathbf{X_S} + \mathbf{u_S} - \sum_{i=1}^{n_{facet}} N_i(\mathbf{X_i} + \mathbf{u_i})) \cdot \mathbf{t}. \tag{2.4}$$

By using equations (2.3) and (2.4), the derivatives for the contact force calculation can be calculated as follows:

$$\frac{\partial g_n}{\partial \mathbf{u_c}} = \frac{\partial(\mathbf{x_S} - \mathbf{x_{TS}})}{\partial \mathbf{u_c}} \cdot \mathbf{n} + (\mathbf{x_S} - \mathbf{x_{TS}}) \cdot \frac{\partial \mathbf{n}}{\partial \mathbf{u_c}}, \tag{2.5}$$

$$\frac{\partial g_t}{\partial \mathbf{u_c}} = \frac{\partial(\mathbf{x_S} - \mathbf{x_{TS}})}{\partial \mathbf{u_c}} \cdot \mathbf{t} + (\mathbf{x_S} - \mathbf{x_{TS}}) \cdot \frac{\partial \mathbf{t}}{\partial \mathbf{u_c}}. \tag{2.6}$$

For deformations where the unit normal (tangential) vector change is negligible, further simplifications are possible. These simplifications are assumed as a result of the stability requirements of the central difference scheme, which require extremely small time steps during the solution.

$$\frac{\partial g_n}{\partial \mathbf{u_c}} \cong \frac{\partial(\mathbf{x_S} - \mathbf{x_{TS}})}{\partial \mathbf{u_c}} \cdot \mathbf{n} = \begin{bmatrix} \mathbf{n} \\ -N_1\mathbf{n} \\ \\ -N_{n_{\text{facet}}}\mathbf{n} \end{bmatrix}, \tag{2.7}$$

$$\frac{\partial g_t}{\partial \mathbf{u_c}} \cong \frac{\partial(\mathbf{x_S} - \mathbf{x_{TS}})}{\partial \mathbf{u_c}} \cdot \mathbf{t} = \begin{bmatrix} \mathbf{t} \\ -N_1\mathbf{t} \\ \\ -N_{n_{\text{facet}}}\mathbf{t} \end{bmatrix}.$$

By using expressions (2.7), the internal contact force vector (2.2) can be easily calculated.

The above derivation corresponds to sticking contact. If friction has to be considered between the surfaces in contact, a Coulomb plasticity model extends the contact force derivation, which is briefly outlined in Appendix D.

2.2. **Multi-surface plasticity model.** In the calculation, a classical multi-surface plasticity theory was utilized in the material model derivation [2], [3]. The following section briefly outlines the essentials of the non-associative multi-surface plasticity model, while a detailed derivation can be found for the combined Mohr-Coulomb and Rankine model in Appendices A-C.

2.2.1. *Plastic velocity strain.* The evolution of plastic velocity strain for non-associative multi-surface plasticity is defined as:

$$\mathbf{D}^{\mathrm{p}} = \sum_{\alpha=1}^{m} \dot{\gamma}^{\alpha} \cdot \partial_{\boldsymbol{\sigma}} \mathrm{r}_{\alpha}(\boldsymbol{\sigma}, \mathbf{q}) \,, \tag{2.8}$$

where $\dot{\gamma}^{\alpha}, \mathrm{r}_{\alpha}(\boldsymbol{\sigma}, \mathbf{q})$ are an unknown plastic multiplier and the non-associative plastic potential function, respectively.

The evolution equations for the hardening variables can be described according to the following formula:

$$\dot{\mathbf{q}} = -\sum_{\alpha=1}^{\mathrm{m}} \dot{\gamma}^{\alpha} \cdot \mathbf{h}_{\alpha}(\boldsymbol{\sigma}, \mathbf{q}), \tag{2.9}$$

where $\mathbf{h}_{\alpha}(\boldsymbol{\sigma}, \mathbf{q}) = \frac{\partial \mathbf{q}}{\partial \gamma^{\alpha}} = \frac{\partial \dot{\mathbf{q}}}{\partial \dot{\gamma}^{\alpha}}$ contains the instantaneous hardening modulus.

2.2.2. *Complementary and consistency requirements.* The complementary conditions state the requirements for the plastic multiplier γ^{α} calculation, and define the admissible stress space $\mathbb{J}_{\mathrm{adm}} := \{\beta \in [1,2,....,\mathrm{m_{adm}}] | \mathrm{f}_{\beta}(\boldsymbol{\sigma},\mathbf{q}) \leqslant 0\}$, respectively for the stress calculation as follows:

$$\text{For} \qquad \alpha = 1,2,...\mathrm{m}, \qquad \gamma^{\alpha} \geqslant 0, \qquad \mathrm{f}_{\alpha}(\boldsymbol{\sigma},\mathbf{q}) \leqslant 0. \tag{2.10}$$

2.2.3. *The consistency requirement summarize the complementary requirements in a short form with the following formula:*

$$\text{For} \qquad \alpha = 1,2,...\mathrm{m}, \qquad \gamma^{\alpha} \cdot \mathrm{f}_{\alpha}(\boldsymbol{\sigma},\mathbf{q}) \equiv 0. \tag{2.11}$$

2.2.4. *Plastic multiplier calculation.* The active stress space condition $\mathbb{J}_{\mathrm{act}} := \{\beta \in \mathbb{J}_{\mathrm{adm}} | \dot{\mathrm{f}}_{\beta}(\boldsymbol{\sigma},\mathbf{q}) = 0\}$ implies the following formulation for the plastic multiplier calculation:

$$\text{For } \alpha = 1,2,...\mathrm{m_{adm.}},$$
$$\mathrm{f}_{\alpha}(\boldsymbol{\sigma},\mathbf{q}) = 0; \quad \dot{\mathrm{f}}_{\alpha}(\boldsymbol{\sigma},\mathbf{q}) = 0 \Rightarrow \sum_{\beta \in \mathbb{J}_{\mathrm{adm}}} \mathrm{g}_{\alpha\beta}(\boldsymbol{\sigma},\mathbf{q}) \cdot \dot{\gamma}^{\beta} = \partial_{\boldsymbol{\sigma}} \mathrm{f}_{\alpha}(\boldsymbol{\sigma},\mathbf{q}) : \mathbf{C}^{\sigma G}_{el} : \mathbf{D}, \tag{2.12}$$

$$\mathrm{g}_{\alpha\beta}(\boldsymbol{\sigma},\mathbf{q}) = \partial_{\boldsymbol{\sigma}} \mathrm{f}_{\alpha}(\boldsymbol{\sigma},\mathbf{q}) : \mathbf{C}^{\sigma G}_{el} : \partial_{\boldsymbol{\sigma}} \mathrm{r}_{\beta}(\boldsymbol{\sigma},\mathbf{q}) + \partial_{\mathbf{q}} \mathrm{f}_{\alpha}(\boldsymbol{\sigma},\mathbf{q}) \cdot \mathbf{h}_{\beta}(\boldsymbol{\sigma},\mathbf{q}).$$

Equation (2.12) represents a system of $\alpha = \mathrm{m_{act}}$ equations with $\alpha = \mathrm{m_{act}}$ unknowns whose solution for the plastic multipliers implies:

$$\dot{\gamma}^{\beta} = 0\,, \qquad \text{if} \qquad \beta \notin \mathbb{J}_{\mathrm{act}}\,, \tag{2.13}$$

$$\dot{\gamma}^{\alpha} = \sum_{\beta \in \mathbb{J}_{\mathrm{act}}} \mathrm{g}^{\alpha\beta}(\boldsymbol{\sigma},\mathbf{q}) \cdot [\partial_{\boldsymbol{\sigma}} \mathrm{f}_{\beta}(\boldsymbol{\sigma},\mathbf{q}) : \mathbf{C}^{\sigma G}_{el} : \mathbf{D}], \qquad \text{if} \qquad \alpha \in \mathbb{J}_{\mathrm{act}}\,, \tag{2.14}$$

where: $\mathrm{g}^{\alpha\beta}(\boldsymbol{\sigma},\mathbf{q})$ are the components of the $[g_{\alpha\beta}(\boldsymbol{\sigma},\mathbf{q})]^{-1}$ tensor.

2.2.5. *Elastic-plastic tangent modulus.* The elastic-plastic tangent modulus can be calculated by back substitution for $\dot{\gamma}^{\alpha}$ as follows:

$$\mathbf{C}^{\sigma G}_{ep} = \mathbf{C}^{\sigma G}_{el} - \sum_{\alpha,\beta \in \mathbb{J}_{\mathrm{act}}} \mathrm{g}^{\alpha\beta}(\boldsymbol{\sigma},\mathbf{q}) [\mathbf{C}^{\sigma G}_{el} : \partial_{\boldsymbol{\sigma}} \mathrm{r}_{\alpha}(\boldsymbol{\sigma},\mathbf{q})] \otimes [\mathbf{C}^{\sigma G}_{el} : \partial_{\boldsymbol{\sigma}} \mathrm{f}_{\beta}(\boldsymbol{\sigma},\mathbf{q})], \quad \text{if} \quad \mathbb{J}_{\mathrm{act}} \neq 0 \tag{2.15}$$

or

$$\mathbf{C}^{\sigma G}_{ep} = \mathbf{C}^{\sigma G}_{el}, \qquad \text{if} \quad \mathbb{J}_{\mathrm{act}} = 0. \tag{2.16}$$

Note: If $\mathbf{h}_{\beta}(\boldsymbol{\sigma},\mathbf{q}) \neq const$, then the system of equations (2.12) is non-linear and iterations are needed to calculate the value of the plastic multiplier. The elastic-plastic tangent modulus is then calculated as $\mathbf{C}^{\sigma G}_{ep} = \frac{\partial \dot{\boldsymbol{\sigma}}}{\partial \mathbf{D}}$, after back substitution for the plastic multiplier in $\dot{\boldsymbol{\sigma}}$.

2.3. **Stress update.** Due to the non-objectivity of the stress measure used in the updated Lagrange formulation, the stress update uses the Green-Naghdi objective rate

$$\boldsymbol{\sigma}^{\nabla G} = \frac{D\boldsymbol{\sigma}}{Dt} - \boldsymbol{\Omega}.\boldsymbol{\sigma} - \boldsymbol{\sigma}.\boldsymbol{\Omega}^{\mathrm{T}} = \mathbf{R}.\frac{D\boldsymbol{\sigma}}{Dt}.\mathbf{R}^{\mathrm{T}} \ , \tag{2.17}$$

which after the numerical integration at the midpoint of the time increment can be expressed in the elastic case as

$$\boldsymbol{\sigma}^{t_n+\Delta t} = \mathbf{R}^{t_n+\Delta t} \cdot \left[\mathbf{C}_{el}^{\sigma G} : \left(\mathbf{R}^{(t_n+\frac{\Delta t}{2})^{\mathrm{T}}} \cdot \mathbf{D}^{(t_n+\frac{\Delta t}{2})} \cdot \mathbf{R}^{(t_n+\frac{\Delta t}{2})} \right) \Delta t + \right.$$
$$\left. + \mathbf{R}^{t_n^{\mathrm{T}}} \cdot \boldsymbol{\sigma}^{t_n} \cdot \mathbf{R}^{t_n} \right] \cdot \mathbf{R}^{t_n+\Delta t^{\mathrm{T}}} \ , \tag{2.18}$$

and in the plastic case as

$$\boldsymbol{\sigma}^{t_n+\Delta t} = \mathbf{R}^{t_n+\Delta t} \cdot \left[\mathbf{C}_{el}^{\sigma G} : \left(\mathbf{R}^{(t_n+\frac{\Delta t}{2})^{\mathrm{T}}} \cdot (\mathbf{D}^{(t_n+\frac{\Delta t}{2})} - \mathbf{D}^{p(t_n+\frac{\Delta t}{2})}) \cdot \mathbf{R}^{(t_n+\frac{\Delta t}{2})} \right) \Delta t + \right.$$
$$\left. + \mathbf{R}^{t_n^{\mathrm{T}}} \cdot \boldsymbol{\sigma}^{t_n} \cdot \mathbf{R}^{t_n} \right] \cdot \mathbf{R}^{t_n+\Delta t^{\mathrm{T}}}, \tag{2.19}$$

where

$$\hat{\mathbf{D}}^{p(t_n+\frac{\Delta t}{2})} = \mathbf{R}^{(t_n+\frac{\Delta t}{2})^{\mathrm{T}}} \mathbf{D}^{p(t_n+\frac{\Delta t}{2})} \mathbf{R}^{(t_n+\frac{\Delta t}{2})} = \sum_{\alpha=1}^{m} \gamma^{\alpha} \cdot \partial_{\boldsymbol{\sigma}} \mathrm{r}_{\alpha} \left(\hat{\boldsymbol{\sigma}}^{t_n+\Delta t}, \hat{\mathbf{q}}^{t_n+\Delta t} \right) \tag{2.20}$$

is a co-rotational plastic velocity strain, $\hat{\sigma}^{t_n+\Delta t}, \hat{\mathbf{q}}^{t_n+\Delta t}$ and $\mathbf{R}$ stand for the co-rotational Cauchy stress, the co-rotational vector of hardening variables and the rotation tensor, respectively.

2.4. **Fracturing.** Mode I fracturing is present only in the Rankine plastic corner. If the first principal plastic strain value reaches the critical fracturing strain value $\varepsilon_c^f = \frac{\mathrm{f_t}}{\mathrm{H}}$, the fracture is inserted. The most meaningful quasi-brittle damage indicator or so-called failure factor is the ratio of the inelastic fracturing strain ε^f to the critical fracturing strain ε_c^f. The local fail factor F_k at Gauss point k is given by

$$F_k = \left(\varepsilon^f / \varepsilon_c^f \right)_k . \tag{2.21}$$

The weighted-average failure factor $\bar{F}_p$ and fracture direction $\bar{\theta}_p$ at node p are given by

$$\bar{F}_p = \sum_{k=1}^{N_{adj}} F_k w_k \Bigg/ \sum_{k=1}^{N_{adj}} w_k, \tag{2.22}$$

$$\bar{\theta}_k = \sum_{k=1}^{N_{adj}} \theta_k w_k \Bigg/ \sum_{k=1}^{N_{adj}} w_k, \tag{2.23}$$

where N_{adj} is the number of immediately adjacent Gauss points and w_k is a weighting factor usually taken as the element volume. The fracture direction angle is allowed to change during the whole period of softening as far as the fracture is inserted. That

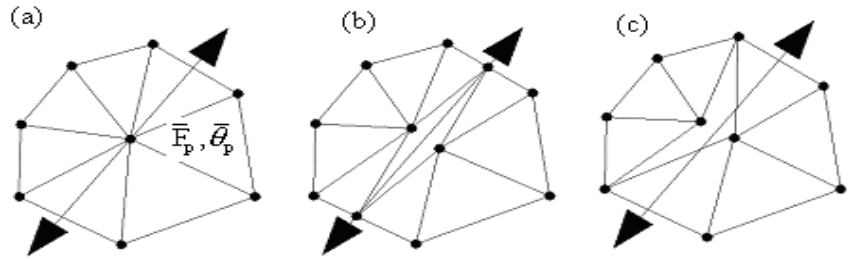

Figure 2. (a) Weighted-average nodal failure direction (b)Intra-element fracturing (c) Inter-element fracturing

is why this kind of fracturing is designated as the rotating crack model. Contact damping can be used on the border between the bodies in contact as a further improvement. The solution uses the modified central difference scheme [4], whose stability sets severe criteria on the time step value.

3. **Simulation of real caving**

There are several material models which treat the discontinuities by introducing various parameters and do the stress update as in the classical plasticity formulation limited to the FEM formulation. All of these models however assume homogenous discontinuity distribution within the element. In rock fracturing this assumption is not necessarily correct [7], [8]. Figure 3 depicts a typical sample of a rock block in reality, its approximated geometry and the further simplified model geometry using two sets of discontinuities. By using the DEM, the above problem can easily be avoided by combining the classical model with homogenous discontinuities and the real discontinuities as shown in Figure 3b,c. One such typical application of the method is the Block caving method, where, during the mining, large blocks of the mined rock fracture into small pieces and flow as a result of the gravity forces. The flow itself is initiated by the material integrity weakening of a supporting layer under the mined rock by its gradual drilling and blasting.

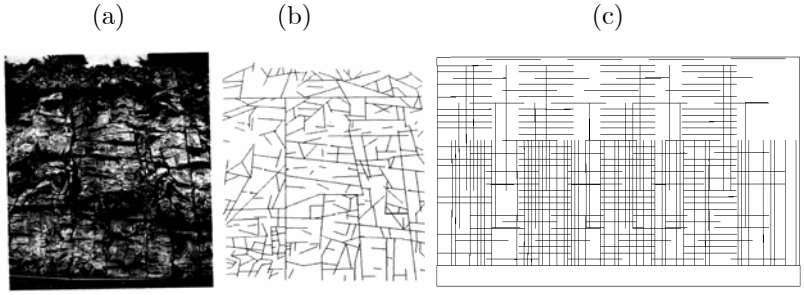

Figure 3. (a) Real geometry, (b) Approximated geometry, (c) Model geometry

3.1. **Description of the numerical model.** The 2D plane-strain model represents a 200m x 100m rock block with two sets of discontinuities. The vertical set is composed of 60m long discontinuities (persistence), with 30m spacing along the discontinuity between the adjacent ends (bridges) and 2m spacing (spacing) in the perpendicular direction between the adjacent discontinuities. The corresponding horizontal set can be described by the following parameters: persistence x bridges x spacing = 30m x 15m x 3m. The caving initialization is realized by a gradual deactivation of supporting elements at the bottom of the model by 10m increments in both directions from the midline of the model. The model uses one Gauss point triangular elements with linear shape functions. The triangular element is advantageous in fracturing, since during the fracturing only further triangular elements can be created, which is a huge simplification and which significantly speeds up the calculation. However, this type of element has an obvious drawback, namely its poor performance in high stress gradient areas.

4. **Numerical Results**

4.1. **Material parameters and loading.** The material properties [9], [10] used in the calculation are based on the real data obtained from the South-African Palabora copper mine and shown in the following Table:

Material property / loadings:	**Value:**
Young's modulus	60 GPa
Poisson's ratio	0.25
Density	3100 kg/m^3
Cohesion stress	8 MPa
Friction angle	55 deg.
Dilatancy angle	9 deg.
Tension cut off stress	1MPa
Fracture energy	70 N/m
Friction angle (between the joints)	33 deg.
Cohesion stress (between the joints)	50 000 Pa
Surface contact damping coefficient	0.5
Model size:	200 x 100 m,
Face loading	15.2 MPa
Body force	30.41 kN/ m^3

Table 1. Material properties of the caved rock

Figure 4 shows the first principal stress distribution which controls the fracturing. The undercut was gradually increased up to 160m. There is no restriction on the flow, the material is allowed to fall freely. In the caved area the lowered density as a result of increasing void ratio can be seen. The numerical simulation shows the extensive fracturing in the caving zone above the undercut area. In mines where the block

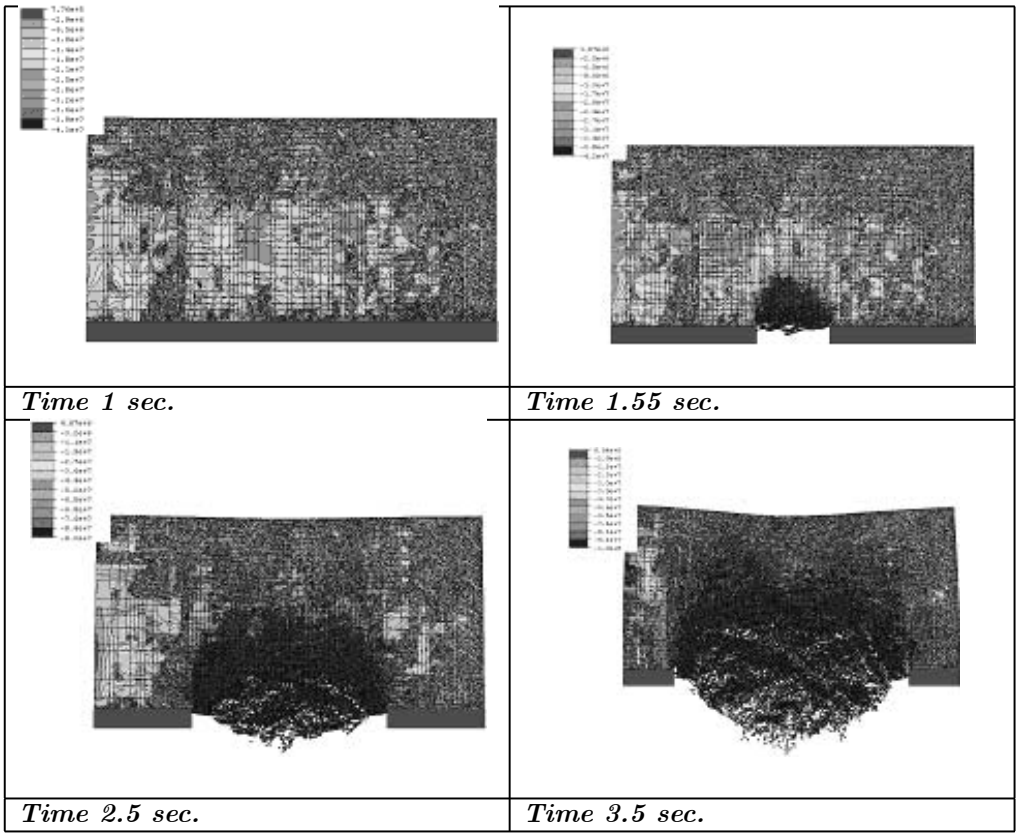

Figure 4. First principal stress distribution

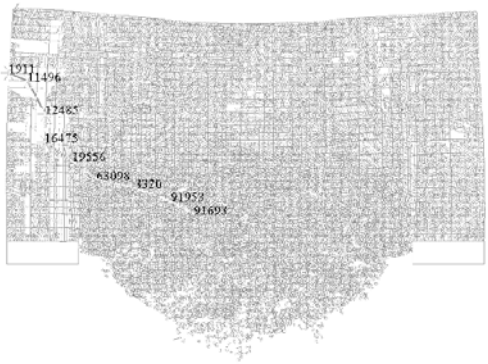

Figure 5. Continuum caving scenario with fracturing at 3.5 sec

caving method is employed, the same effect was observed, as there were not any extremely large pieces of rocks on the operation level during the haulage.

Figure 5 shows the fractured rock flow at time 3.5 sec.

4.2. **Stress states at selected points.** The following Table shows some typical stress values for the selected points in Figure 5 at time 3.5 sec.

	x [m]	y [m]	σ_{xx} [MPa]	σ_{yy} [MPa]	σ_{zz} [MPa]	σ_{xy} [MPa]
Node 91693	77.58	-533.76	-1.298	-1.107	-0.792	-0.611
Node 91953	67.44	-529.09	0.011	0.074	-0.335	0.087
Node 3320	51.00	-520.00	-1.535	0.015	-0.236	-0.613
Node 63098	38.20	-520.40	-9.079	-5.526	-3.651	-6.747
Node 19556	27.71	-514.65	-9.312	-34.463	-10.944	-12.985
Node 16475	16.00	-507.00	-20.551	-51.560	-18.028	-10.029
Node 12485	16.00	-495.00	-30.486	-63.564	-23.512	3.075
Node 11496	8.00	-481.00	-23.092	-17.362	-10.113	3.266
Node 1911	0.00	-478.00	-21.642	-0.274	-5.479	1.536

Table 2. Stress values at selected nodes

5. **Conclusion**

The biggest advantage of the method presented is the ability to model extensive fracturing. The method allows us to model situations where the conventional finite element method would fail. The calculation uses explicit dynamic formulation of equations of motion and the combined Mohr-Coulomb and Rankine plasticity model with mode I fracturing based on the rotating crack model. Due to the stability requirements and the extensive contact search between the discrete bodies, even 2D calculations with a relatively small number (several ten thousands) of elements appear to be very expensive. A similar 3D simulation without sorting out the parallel processing of the code is thus unimaginable.

Acknowledgement. Funding provided by Rio Tinto and VEGA SR is gratefully acknowledged.

REFERENCES

1. Belytschko, T., Wam Kam Lui and Moran, B.: *Nonlinear Finite Element Analysis for Continua and Structures.* Chichester, John Wiley & Sons, 1999.
2. Hinton, E. and Owen, R.: *Computational Modelling of Reinforced Concrete Structures.* Swansea, Pineridge Press, 1986.
3. Simo, J. C. and Hughes, J. R.: *Computational Inelasticity.* New York, Springer-Verlag, 1998.
4. Cook, R. D., Malkus, D. S., and Plesha, M. E.: *Concepts and Applications of Finite Element Analysis*, New York, N.Y., John Wiley & Sons, 1989.

5. Clerk, P. A.: *The Finite Element Modelling of Discrete Fracture in Quasi-Brittle Materials*. Thesis, Dept. of Civil Engineering, UW Swansea, 2000.
6. Yu, J. G.: *A contact interaction framework for numerical simulation of multi body problems and aspects of damage and fracture for brittle materials*. Thesis, Dept. of Civil Engineering, UW Swansea, 1995.
7. Tinto R.: *Caving Study*. End of Project Report, Nov. 1997 to Nov. 2000.
8. Brady, B. H. G. and Brown, E. T.: *Rock mechanics for underground mining*, 2nd. edition, Chapman & Hall, 1993
9. Peter, J. and Gash S.: *In situ stress measurement*. Palabora Underground Mining Project, 1999.
10. Itasca Consulting Group, *Examination of the Caving Potential for the Palabora Underground Mine*, Internal report, 1995.
11. Bazant, Z. P. and Planas, J.: *Fracture and size effect in concrete and other quasibrittle materials*, CRC Press LLC, 1998.

Appendix A

In the sequel we briefly outline the combined Mohr-Coulomb and Rankine plasticity model. Depending on which part of the plasticity surface is active the following possibilities can be distinguished.

A.1. **Mohr-Coulomb constitutive model.** The Mohr-Coulomb plasticity surface usually becomes active if the principal stresses are compressive. As a simplification perfect plasticity was considered, which means the plasticity surface is static. The following cases can be distinguished and are depicted in the π - plane (Figure 6):

If $\sigma_1 \geqslant \sigma_2 \geqslant \sigma_3$ are the principal stresses and c_0, φ, ψ are the cohesion stress, friction angle and dilatation angle, the plasticity surface equation is given as follows:

$$\frac{1}{2}(\sigma_1 - \sigma_3) + \frac{1}{2}(\sigma_1 + \sigma_3)\sin\varphi = c_0 \cos\varphi \tag{A.1}$$

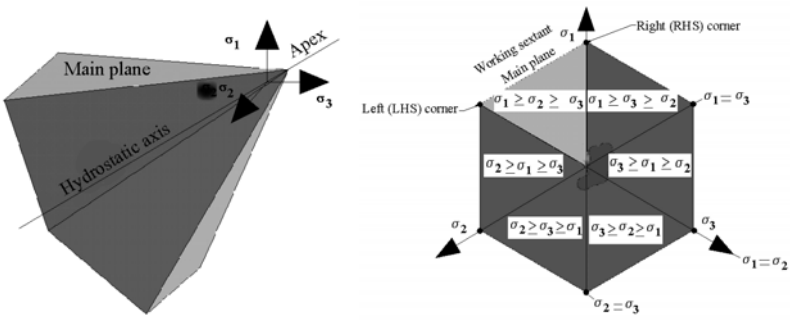

Figure 6. (a) The 3D Mohr-Coulomb yield-surface in principal stress spaces (b) The π-plane representation

- *Plastic flow from the main plane.* This is the simplest case, depicted in Figure 7. The trial stress crosses only one stress space, and only this stress space is active at one time. The active stress space is given by function f_1, the plastic potential function by r_1 and the hardening variables by h_1.

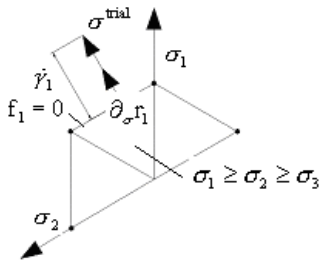

Figure 7. Main plane plasticity flow representation

$$\mathrm{m}_{\mathrm{act}} = 1, \quad \mathrm{f}_1 = \tfrac{1}{2}(\sigma_1 - \sigma_3) + \tfrac{1}{2}(\sigma_1 + \sigma_3)\sin\varphi - c_o\cos\varphi = 0 \tag{A.2a}$$

$$\mathrm{r}_1 = \tfrac{1}{2}(\sigma_1 - \sigma_3) + \tfrac{1}{2}(\sigma_1 + \sigma_3)\sin\psi - c_o\cos\psi = 0 \tag{A.2b}$$

For $c_o = const$, $\varphi = const$ and $\psi = const$- these conditions ensure that the plasticity surface is static.

$$\mathbf{q}^T = [\ c_0 \quad \varphi \quad \psi\ ] \quad - \text{vector of state variables}, \quad \mathbf{h}_1^T = [\ 0 \quad 0 \quad 0] \tag{A.2c}$$

- *Plastic flow from the right corner (RHS)* The corner points represent the state where a number of stress spaces might be active at one time. At the right corner (Fig. 8) two stress spaces are active given by functions $\mathrm{f}_1, \mathrm{f}_2$, the plastic potential functions are given by $\mathrm{r}_1, \mathrm{r}_2$ and the hardening variables by $\mathrm{h}_1, \mathrm{h}_2$.

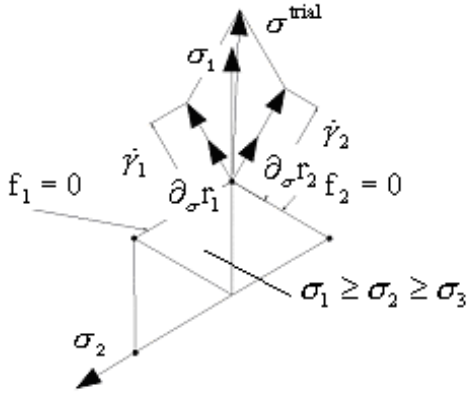

Figure 8. Right corner plasticity flow representation

$$\mathrm{m}_{\mathrm{act}} = 2, \quad \mathrm{f}_1 = \tfrac{1}{2}(\sigma_1 - \sigma_3) + \tfrac{1}{2}(\sigma_1 + \sigma_3)\sin\varphi - c_o\cos\varphi = 0 \tag{A.3a}$$

$$\mathrm{r}_1 = \tfrac{1}{2}(\sigma_1 - \sigma_3) + \tfrac{1}{2}(\sigma_1 + \sigma_3)\sin\psi - c_o\cos\psi = 0 \tag{A.3b}$$

$$\mathrm{f}_2 = \tfrac{1}{2}(\sigma_1 - \sigma_2) + \tfrac{1}{2}(\sigma_1 + \sigma_2)\sin\varphi - c_o\cos\varphi = 0 \tag{A.3c}$$

$$\mathrm{r}_2 = \tfrac{1}{2}(\sigma_1 - \sigma_2) + \tfrac{1}{2}(\sigma_1 + \sigma_2)\sin\psi - c_o\cos\psi = 0 \tag{A.3d}$$

for $c_o = const$, $\varphi = const$ and $\psi = const$

$$\mathbf{q}^T = [\ c_0 \quad \varphi \quad \psi\ ],\ \ \mathbf{h}_1^T = \mathbf{h}_2^T = [\ 0 \quad 0 \quad 0] \tag{A.3e}$$

- *Plastic flow from the left corner (LHS)* It is analogous to the plastic flow from the right corner (Figure 9).

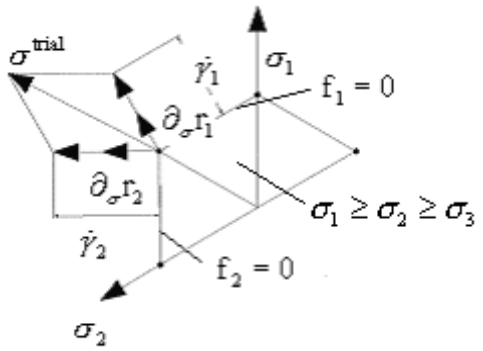

Figure 9. Left corner plasticity flow representation

$$\mathrm{m_{act}} = 2, \quad \mathrm{f}_1 = \tfrac{1}{2}(\sigma_1 - \sigma_3) + \tfrac{1}{2}(\sigma_1 + \sigma_3)\sin\varphi - c_o\cos\varphi = 0 \tag{A.4a}$$

$$\mathrm{r}_1 = \tfrac{1}{2}(\sigma_1 - \sigma_3) + \tfrac{1}{2}(\sigma_1 + \sigma_3)\sin\psi - c_o\cos\psi = 0 \tag{A.4b}$$

$$\mathrm{f}_2 = \tfrac{1}{2}(\sigma_2 - \sigma_3) + \tfrac{1}{2}(\sigma_2 + \sigma_3)\sin\varphi - c_o\cos\varphi = 0 \tag{A.4c}$$

$$\mathrm{r}_2 = \tfrac{1}{2}(\sigma_2 - \sigma_3) + \tfrac{1}{2}(\sigma_2 + \sigma_3)\sin\psi - c_o\cos\psi = 0 \tag{A.4d}$$

for $c_o = const$, $\varphi = const$ and $\psi = const$

$$\mathbf{q}^T = [\ c_0 \quad \varphi \quad \psi\ ],\ \ \mathbf{h}_1^T = \mathbf{h}_2^T = [\ 0 \quad 0 \quad 0\ ] \tag{A.4e}$$

- *Plastic flow from the apex.* At the apex (Figure 10) two stress spaces corresponding to the hydrostatic and deviatoric stress are active and given by functions $\mathrm{f}_1, \mathrm{f}_2$, as well as the plastic potential functions by $\mathrm{r}_1, \mathrm{r}_2$ and the hardening variables by $\mathrm{h}_1, \mathrm{h}_2$.

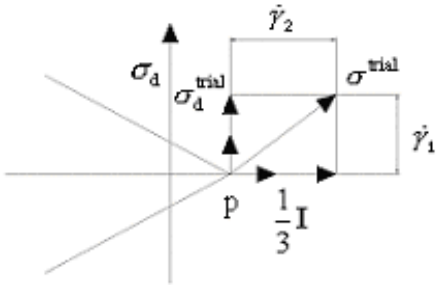

Figure 10. Plastic flow from the apex representation

$$m_{\text{act}} = 2, \quad \text{f}_1 = f_a^{DEV}(\boldsymbol{\sigma}, \varepsilon^p) = \boldsymbol{\sigma}_d = 0, \tag{A.15}$$

$$\text{r}_1 = \text{f}_1; \quad \text{f}_2 = f_b^{HYD}(\boldsymbol{\sigma}, \varepsilon^p) = \text{p} - c_o \cot\varphi = 0; \quad \text{r}_2 = \text{f}_2, \tag{A.16}$$

where $\boldsymbol{\sigma}_d = \text{dev}[\boldsymbol{\sigma}] = \boldsymbol{\sigma} - \text{p}\mathbf{I}$ and $\text{p} = \text{tr}[\boldsymbol{\sigma}] = (\sigma_1 + \sigma_2 + \sigma_3)/3$ for

$$c_o = const\,, \quad \varphi = const; \quad \mathbf{q}^T = [\ c_0 \quad \varphi\ ]\,, \quad \mathbf{h}_1^T = \mathbf{h}_2^T = [\ 0 \quad 0\ ]. \tag{A.17}$$

Appendix B. Rankine constitutive model

The Rankine failure model (Figure 11) governs the failure of brittle material in tension. When fracturing is considered, the FEM applications usually distinguish between the so-called fixed and rotating crack models.

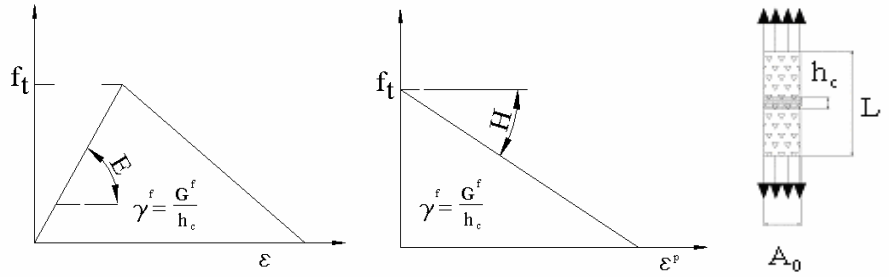

Figure 11. a) Stress strain curve, b) Stress plastic strain curve, c) Uniaxial specimen with crack band

The material behavior and the first principal stress value on the element level, is linear up to the so-called uniaxial tension strength, then it softens as is shown in Figure 11. The fixed crack model direction remains fixed after the peak value of the first principal stress has been reached, while in the case of the rotating crack model the fracture angle is allowed to change while the material softens as far as the crack is inserted.

$$\text{If } \sigma_1 \geqslant \sigma_2 \geqslant \sigma_3\,;\ \text{m}_{\text{act}} = 1\,;\ \text{f}_1 = \sigma_1 - \sigma_y(\varepsilon^p) = 0\,;\ \text{r}_1 = \text{f}_1; \tag{B.1}$$

$$\frac{\partial\varepsilon(\gamma^1)^p}{\partial\gamma^1} = 1, \quad q = \sigma_y(\varepsilon^p); \quad h_1(\boldsymbol{\sigma}, q) = h_1(\boldsymbol{\sigma}, \varepsilon^p) = \frac{\partial\sigma_y}{\partial\varepsilon^p} \cdot \frac{\partial\varepsilon^p}{\partial\gamma^1} = -\text{H}. \tag{B.2}$$

Evolution of the tensile strength:

$$\sigma_y = \sigma_y(\varepsilon^p) = f_t - H\varepsilon^p\,. \tag{B.3}$$

From the equivalence of the area, which represents the fracture energy per unit length to create a crack surface of uniform area, the softening modulus can be calculated as follows:

$$\frac{1}{2}\cdot\frac{\mathrm{f}_t^2}{\mathrm{H}}=\frac{\mathrm{G}_f}{\mathrm{h}_c^{(e)}}\Rightarrow\quad \mathrm{H}=-\frac{\mathrm{d}\sigma_y}{\mathrm{d}\varepsilon^p}=\frac{\mathrm{h}_c^{(e)}\cdot\mathrm{f}_t^2}{2\cdot\mathrm{G}_f} \tag{B.4}$$

where

$$\mathrm{h}_\mathrm{c}^{(\mathrm{e})}\approx\sqrt{4A^{(e)}/\pi}\qquad\text{for 2 - D triangular elements and} \tag{B.5a}$$

$$\mathrm{h}_\mathrm{c}^{(\mathrm{e})}\approx\sqrt[3]{6V^{(e)}/\pi}\qquad\text{for 3 - D tetrahedral elements.} \tag{B.5b}$$

It is assumed, that the micro cracks in the fracture process zone are distributed over a band of width h (Figure 11c), hence the name crack band model (CBM). The technique, where the deformations are smeared over the element is called the smeared crack approach. In the FEM application the following technique was used for the equivalent crack band calculation (See Figure 12 and equations (B.5)).

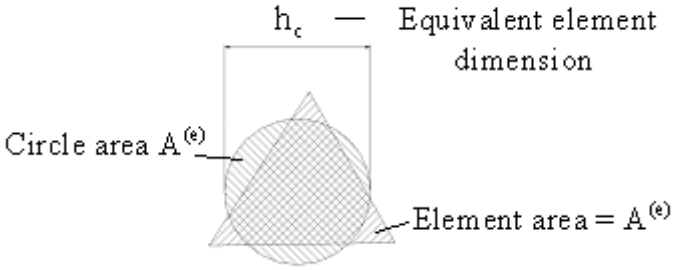

Figure 12. The approximate (equivalent) element dimension for a plane triangular element

Appendix C. Combined Mohr-Coulomb and Rankine constitutive model

It describes the plastic behavior of the model at the places where the Mohr-Coulomb and Rankine plasticity surfaces intersect each other (see Figure 13). As can be seen in the Figure, in compression there is always a stress space where the material remains elastic.

Single vector return mapping to the σ_1 tensile plane (for the interior of the ACD triangle see Figure 13): It is analogous to the Rankine constitutive model.

Two vector return mapping to the intersection of the σ_1 and σ_2 tensile planes (for the interior of the AD line see Figure 13) In the tensile corner it is assumed that the yield surfaces are independent of each other so if one surface softens, the remaining one does not change its position.

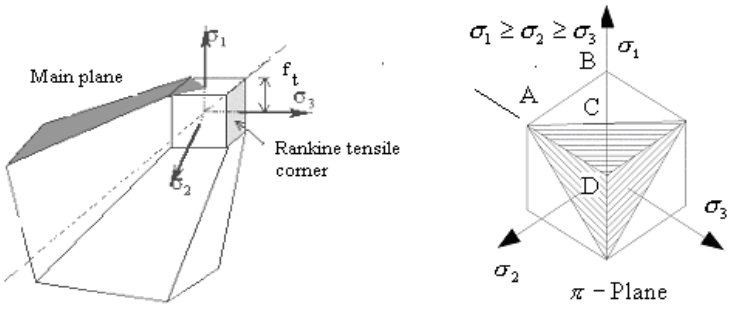

Figure 13. Combined Mohr-Coulomb and Rankine constitutive model representation

$$\mathrm{m_{act}} = 2; \quad \mathrm{f}_1 = \sigma_1 - \sigma_{y1}\left(\varepsilon_1^p\right) = 0; \quad \mathrm{r}_1 = \mathrm{f}_1\,; \quad \mathrm{f}_2 = \sigma_2 - \sigma_{y2}\left(\varepsilon_2^p\right) = 0\,; \quad \mathrm{r}_2 = \mathrm{f}_2; \tag{C.1}$$

$$\frac{\partial \varepsilon_1(\gamma^1)^p}{\partial \gamma^1} = 1\,; \quad \frac{\partial \varepsilon_2(\gamma^2)^p}{\partial \gamma^2} = 1; \quad \sigma_{y1} = \sigma_{y1}\left(\varepsilon_1^p\right) = f_t - H\varepsilon_1^p; \quad \sigma_{y2} = \sigma_{y2}\left(\varepsilon_2^p\right) = f_t - H\varepsilon_2^p; \tag{C.2}$$

$$\mathbf{q}^T = [\ \sigma_{y1} \quad \sigma_{y2}\ ]; \quad \mathbf{h}_1^T = [\ \text{-H} \quad 0\ ]\,; \quad \mathbf{h}_2^T = [\ 0 \quad \text{-H}\ ]. \tag{C.3}$$

Three vector return mapping to the Rankine tensile corner apex (for point D see Figure 13):

$$\mathrm{m_{act}} = 3; \quad \mathrm{f}_1 = \sigma_1 - \sigma_{y1}\left(\varepsilon_1^p\right) = 0; \quad \mathrm{r}_1 = \mathrm{f}_1; \quad \mathrm{f}_2 = \sigma_2 - \sigma_{y2}\left(\varepsilon_2^p\right) = 0; \tag{C.4}$$

$$\mathrm{r}_2 = \mathrm{f}_2; \quad \mathrm{f}_3 = \sigma_3 - \sigma_{y3}\left(\varepsilon_3^p\right) = 0; \quad \mathrm{r}_3 = \mathrm{f}_3; \tag{C.5}$$

$$\frac{\partial \varepsilon_1(\gamma^1)^p}{\partial \gamma^1} = 1\,; \frac{\partial \varepsilon_2(\gamma^2)^p}{\partial \gamma^2} = 1\,; \frac{\partial \varepsilon_3(\gamma^3)^p}{\partial \gamma^3} = 1\,; \quad \sigma_{y1} = \sigma_{y1}\left(\varepsilon_1^p\right) = f_t - H\varepsilon_1^p; \tag{C.6}$$

$$\sigma_{\mathrm{y2}} = \sigma_{\mathrm{y2}}\left(\varepsilon_2^p\right) = f_t - H \cdot \varepsilon_2^p; \quad \sigma_{\mathrm{y3}} = \sigma_{\mathrm{y3}}\left(\varepsilon_3^p\right) = f_t - H \cdot \varepsilon_3^p; \tag{C.7}$$

$$\mathbf{q}^T = [\ \sigma_{y1} \quad \sigma_{y2} \quad \sigma_{y3}\ ]\,; \quad \mathbf{h}_1^T = [\ \text{-H} \quad 0 \quad 0\ ]\,; \tag{C.8}$$

$$\mathbf{h}_2^T = [\ 0 \quad \text{-H} \quad 0\ ]\,; \quad \mathbf{h}_3^T = [\ 0 \quad 0 \quad \text{-H}\ ]. \tag{C.9}$$

Two vector return mapping to the intersection of the Mohr-Coulomb main plane and the σ_1 tensile plane (for the interior of the line AC see Figure 13):

$$\mathrm{m_{act}} = 2; \quad \mathrm{f}_1 = \tfrac{1}{2}\left(\sigma_1 - \sigma_3\right) + \tfrac{1}{2}\left(\sigma_1 + \sigma_3\right)\sin\varphi - c_o\cos\varphi = 0; \quad \mathrm{f}_2 = \sigma_1 - \sigma_y(\varepsilon^p) = 0; \tag{C.10}$$

$$\mathrm{r}_1 = \tfrac{1}{2}\left(\sigma_1 - \sigma_3\right) + \tfrac{1}{2}\left(\sigma_1 + \sigma_3\right)\sin\psi - c_o\cos\psi = 0; \quad \mathrm{r}_2 = \mathrm{f}_2; \tag{C.11}$$

for $c_o = const$, $\varphi = const$ and $\psi = const$. The Mohr-Coulomb plasticity surface does not change:

$$\mathbf{q}^T = [\ c_0 \quad \varphi \quad \psi \quad \sigma_y\varepsilon^p\ ]\,; \ \mathbf{h}_1^T = [\ 0 \quad 0 \quad 0 \quad 0\ ]\,; \ \mathbf{h}_2^T = [\ 0 \quad 0 \quad 0 \quad -\mathrm{H}\ ] \tag{C.12}$$

Three vector return-mapping to the intersection of the right edge of the Mohr-Coulomb main-plane and the σ_1 tensile plane (for point C see Figure 13)

$$\mathrm{m_{act}} = 3; \quad \mathrm{f}_1 = \tfrac{1}{2}(\sigma_1 - \sigma_3) + \tfrac{1}{2}(\sigma_1 + \sigma_3)\sin\varphi - c_o\cos\varphi = 0; \tag{C.13}$$

$$\mathrm{f}_2 = \tfrac{1}{2}(\sigma_1 - \sigma_2) + \tfrac{1}{2}(\sigma_1 + \sigma_2)\sin\varphi - c_o\cos\varphi = 0; \quad \mathrm{f}_3 = \sigma_1 - \sigma_y(\varepsilon^p) = 0; \tag{C.14}$$

$$\mathrm{r}_1 = \tfrac{1}{2}(\sigma_1 - \sigma_3) + \tfrac{1}{2}(\sigma_1 + \sigma_3)\sin\psi - c_o\cos\psi = 0; \tag{C.15}$$

$$\mathrm{r}_2 = \tfrac{1}{2}(\sigma_1 - \sigma_2) + \tfrac{1}{2}(\sigma_1 + \sigma_2)\sin\psi - c_o\cos\psi = 0; \quad \mathrm{r}_3 = \mathrm{f}_3; \tag{C.16}$$

for $c_o = const$, $\varphi = const$ and $\psi = const$

$$\mathbf{q}^T = [\ c_0 \quad \varphi \quad \psi \quad \sigma_y(\varepsilon^p)\ ]; \quad \mathbf{h}_1^T = [\ 0 \quad 0 \quad 0 \quad 0\ ]; \tag{C.17}$$

$$\mathbf{h}_2^T = [\ 0 \quad 0 \quad 0 \quad 0\ ]; \quad \mathbf{h}_3^T = [\ 0 \quad 0 \quad 0 \quad -\mathrm{H}\ ]. \tag{C.18}$$

Four vector return-mapping to the intersection of the left edge of the Mohr-Coulomb main-plane and the σ_1 and σ_2 tensile planes (point A see Figure 13)

$$\mathrm{m_{act}} = 4\,; \ \mathrm{f}_1 = \tfrac{1}{2}(\sigma_1 - \sigma_3) + \tfrac{1}{2}(\sigma_1 + \sigma_3)\sin\varphi - c_o\cos\varphi = 0\,; \tag{C.19}$$

$$\mathrm{f}_2 = \tfrac{1}{2}(\sigma_2 - \sigma_3) + \tfrac{1}{2}(\sigma_2 + \sigma_3)\sin\varphi - c_o\cos\varphi = 0; \quad \mathrm{f}_3 = \sigma_1 - \sigma_{y1}(\varepsilon_1^p) = 0; \tag{C.20}$$

$$\mathrm{f}_4 = \sigma_2 - \sigma_{\mathrm{y}2}(\varepsilon_2^p) = 0; \quad \mathrm{r}_1 = \tfrac{1}{2}(\sigma_1 - \sigma_3) + \tfrac{1}{2}(\sigma_1 + \sigma_3)\sin\psi - c_o\cos\psi = 0\,; \tag{C.21}$$

$$\mathrm{r}_2 = \tfrac{1}{2}(\sigma_2 - \sigma_3) + \tfrac{1}{2}(\sigma_2 + \sigma_3)\sin\psi - c_o\cos\psi = 0; \mathrm{r}_3 = \mathrm{f}_3; \quad \mathrm{r}_4 = \mathrm{f}_4\,; \tag{C.22}$$

$$\mathbf{q}^T = [\ c_0 \quad \varphi \quad \psi \quad \sigma_{y1}(\varepsilon_1^p) \quad \sigma_{y2}(\varepsilon_2^p)\ ]; \quad \mathbf{h}_1^T = [\ 0 \quad 0 \quad 0 \quad 0 \quad 0\ ]; \tag{C.23}$$

$$\mathbf{h}_2^T = [\ 0 \quad 0 \quad 0 \quad 0 \quad 0\ ], \quad \mathbf{h}_3^T = [\ 0 \quad 0 \quad 0 \quad -\mathrm{H} \quad 0\ ], \quad \mathbf{h}_4^T = [\ 0 \quad 0 \quad 0 \quad 0 \quad -\mathrm{H}\ ]. \tag{C.24}$$

Appendix D. Tangential interaction law - The Coulomb friction model

The tangential interaction law describes the friction contact if a friction slip occurs between the bodies. It is formulated as follows:

$$\mathrm{g}_t = \mathrm{g}_t^{\mathrm{e}} + \mathrm{g}_t^p\,; \quad \mathbf{f}_{c_t}^{\mathrm{int}} = \alpha_t \mathrm{g}_t^e \mathbf{t} = \alpha_t\,(\mathrm{g}_t - \mathrm{g}_t^p)\mathbf{t}\,, \tag{D.1}$$

where g_t is the tangential gap and $\mathbf{t}$ is the unit tangential vector at the place of ontact.

The Coulomb friction phenomenon can be described as:

$$\mathrm{f}_1 = \left\|\mathbf{f}_{c_t}^{\mathrm{int}}\right\| - (\mathrm{f}_{c_n}^{\mathrm{int}}\mu + C_0) \leqslant 0\,, \tag{D.2}$$

where μ is the friction coefficient and C_0 is the cohesion force.

The non-associative plastic flow (slip) potential function is:

$$\mathrm{r}_1 = \left\|\mathbf{f}_{c_t}^{\mathrm{int}}\right\|\,; \quad \boldsymbol{\Delta}\mathbf{g}_t^p = \Delta\lambda\,\frac{\partial \mathrm{r}_1}{\partial \mathbf{f}_{c_t}^{\mathrm{int}}} = \Delta\lambda\,\frac{\mathbf{f}_{c_t}^{\mathrm{int}}}{\left\|\mathbf{f}_{c_t}^{\mathrm{int}}\right\|} = \Delta\lambda\mathbf{t}; \quad \Delta\mathrm{f}_{c_n}^{\mathrm{int}} = \alpha_n\,\Delta\mathrm{g}_n \tag{D.3}$$

The slipping/sticking conditions can be formulated in the discrete Kuhn-Tucker form with the following complementary and consistency requirements:

$$\mathrm{f}_1 \leqslant 0, \quad \Delta\lambda \geqslant 0, \quad \Delta\lambda \cdot \mathrm{f}_1 = 0. \tag{D.4}$$